Supplemental Data Information

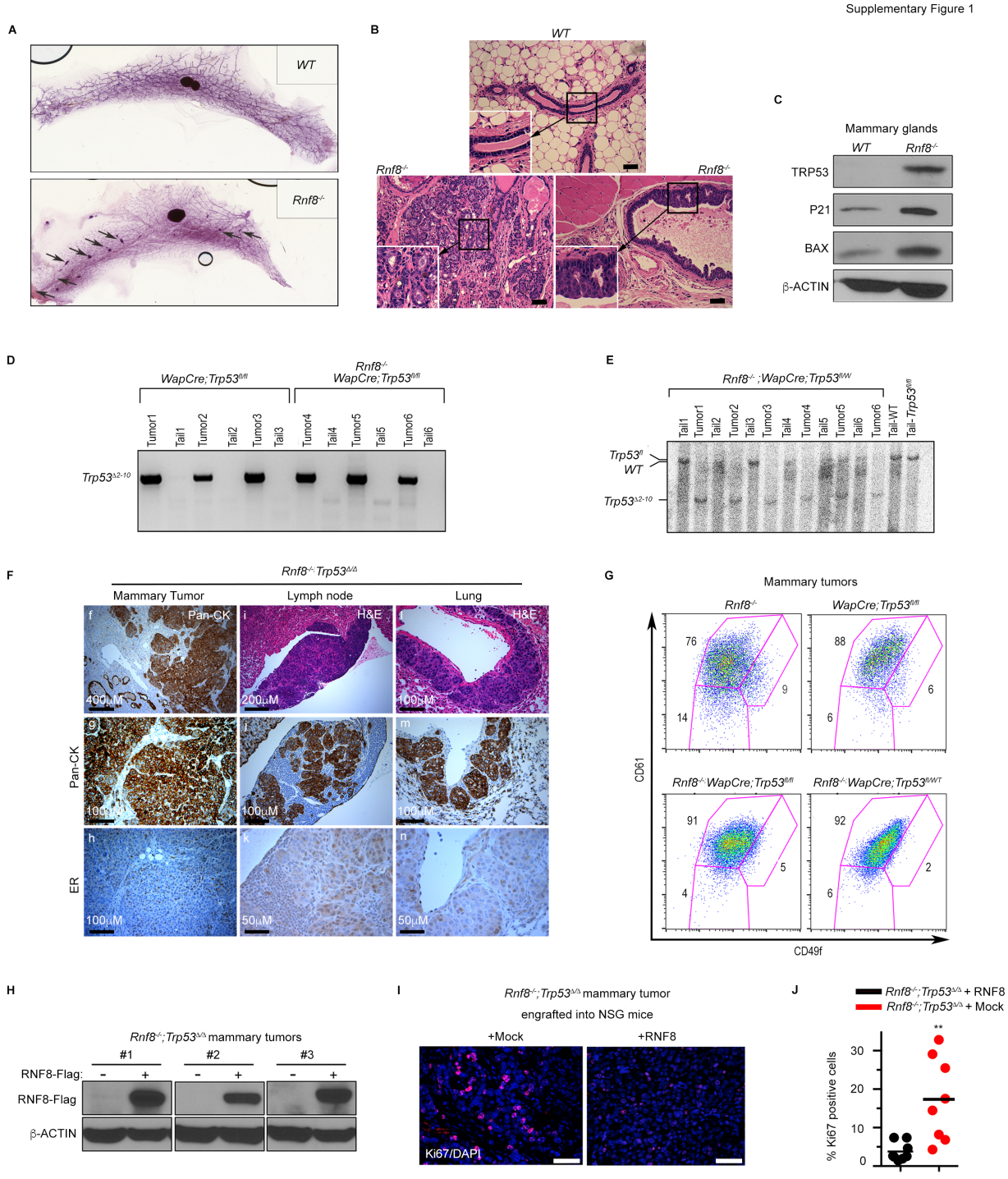

Figure S1. *Rnf8* mutant female mice display increased predisposition for mammary tumorigenesis.

(**A**) Representative images of carmine-alum stained whole mount of inguinal mammary glands from cohorts of 13-month-old *WT* (n=19) and *Rnf8*$^{-/-}$ (n=20) females. Although no hyperplasia was observed in mammary glands of the age-matched *WT* females, mammary glands of *Rnf8*$^{-/-}$ females showed the presence of contained areas of hyperplastic lesions (arrows). (**B**) Representative images of H&E stained axillary mammary glands from at least 5 *WT* and *Rnf8*$^{-/-}$ females from the cohorts in (**A**). Boxed regions are shown at higher magnification. No hyperplasia was observed in mammary glands of the examined *WT* females, however; mammary glands of *Rnf8*$^{-/-}$ females showed the presence of contained areas of typical hyperplasia. Bar: 50μm. (**C**) Representative immunoblots of three independent experiments showing the expression of TRP53, P21 and BAX in mammary glands of one-year-old *WT* and *Rnf8*$^{-/-}$ female littermates. **(D)** Trp53 deletion in mammary tumors from *Rnf8*$^{-/-}$*;WapCre;Trp53*$^{fl/fl}$ and *WapCre;Trp53*$^{fl/fl}$ females. PCR analysis of Trp53-deleted allele (*Trp53*$^{\Delta 2\text{-}10}$) in genomic DNA from tails and mammary tumors of *WapCre;Trp53*$^{fl/fl}$ and *Rnf8*$^{-/-}$*;WapCre;Trp53*$^{fl/fl}$ females. (**E**) Southern blot analysis showing loss of heterozygosity of Trp53 wildtype allele in mammary tumors from *Rnf8*$^{-/-}$*;WapCre;Trp53*$^{fl/WT}$ females. Genomic DNA from tails of the respective tumor bearing females were used as controls. (**F**) Representative staining of at least three independent experiments showing expression of pan-cytokeratin (Pan-CK), and ER staining of *Rnf8*$^{-/-}$*;Trp53*$^{\Delta/\Delta}$ mammary adenocarcinomas and their metastases to lymph nodes and lung as indicated. (**G**) Representative FACS plot analysis of the expression profile of CD49f, and CD61 markers in at least three different mammary tumors from *Rnf8*$^{-/-}$, *WapCre;Trp53*$^{fl/fl}$, *Rnf8*$^{-/-}$*;WapCre;Trp53*$^{fl/fl}$ and *Rnf8*$^{-/-}$*;WapCre;Trp53*$^{fl/WT}$ females. (**H**) Western blot analysis of the expression of exogenous RNF8 in 3 different *Rnf8*$^{-/-}$*;Trp53*$^{\Delta/\Delta}$ mammary tumors complemented with either mock (-) or RNF8^{WT}-Flag (RNF8-Flag). **(I, J**) *Rnf8*$^{-/-}$*;Trp53*$^{\Delta/\Delta}$ mammary tumors cells, and their RNF8 reconstituted controls, were orthotopically injected into inguinal fat pads of NSG mice and tumors were collected 40 days later and stained for Ki67. Representative images are shown (**I**) and dot plots depicts mean ± SEM of Ki67 positive tumor cells resected from 10-12 NSG mice following 40 days of outgrowth (**J**). ** P<0.01, two-sided Student's *t*-test.

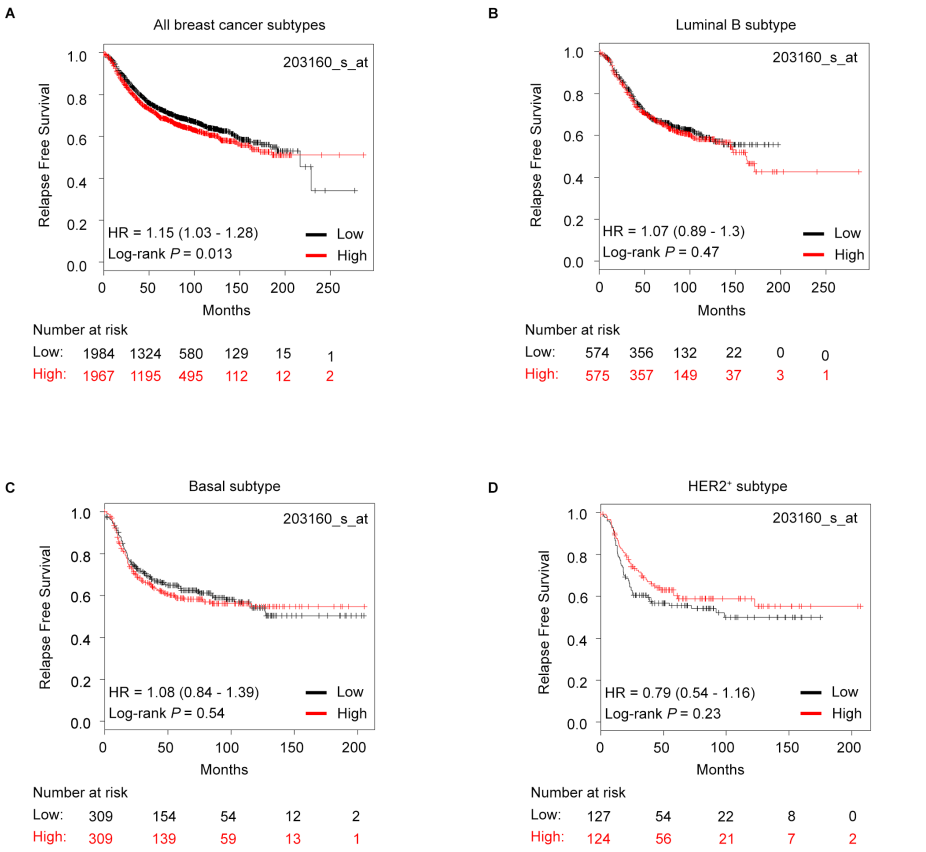

Figure S2. KM plotter analysis for the correlation between *RNF8* 203160_s_at probe and relapse-free survival of breast cancer patients.

Analysis of relapse-free survival of breast cancer patients using KM plotter and the median expression level of *RNF8* 203160_s_at probe to classify cases as either expressing high or low levels. The *RNF8* 203160_s_at probe detects several *RNF8* isoforms predicted to be non-functional (see **Figure 2A**). The analysis included all breast cancer patients (n=3,955), patients with luminal B (n=1,149), basal-like (n=618) or HER2-positive (n=251) subtypes. Hazard ratio (HR) and 95% confidence intervals of the Cox regression analysis, and log-rank *P* values are shown.

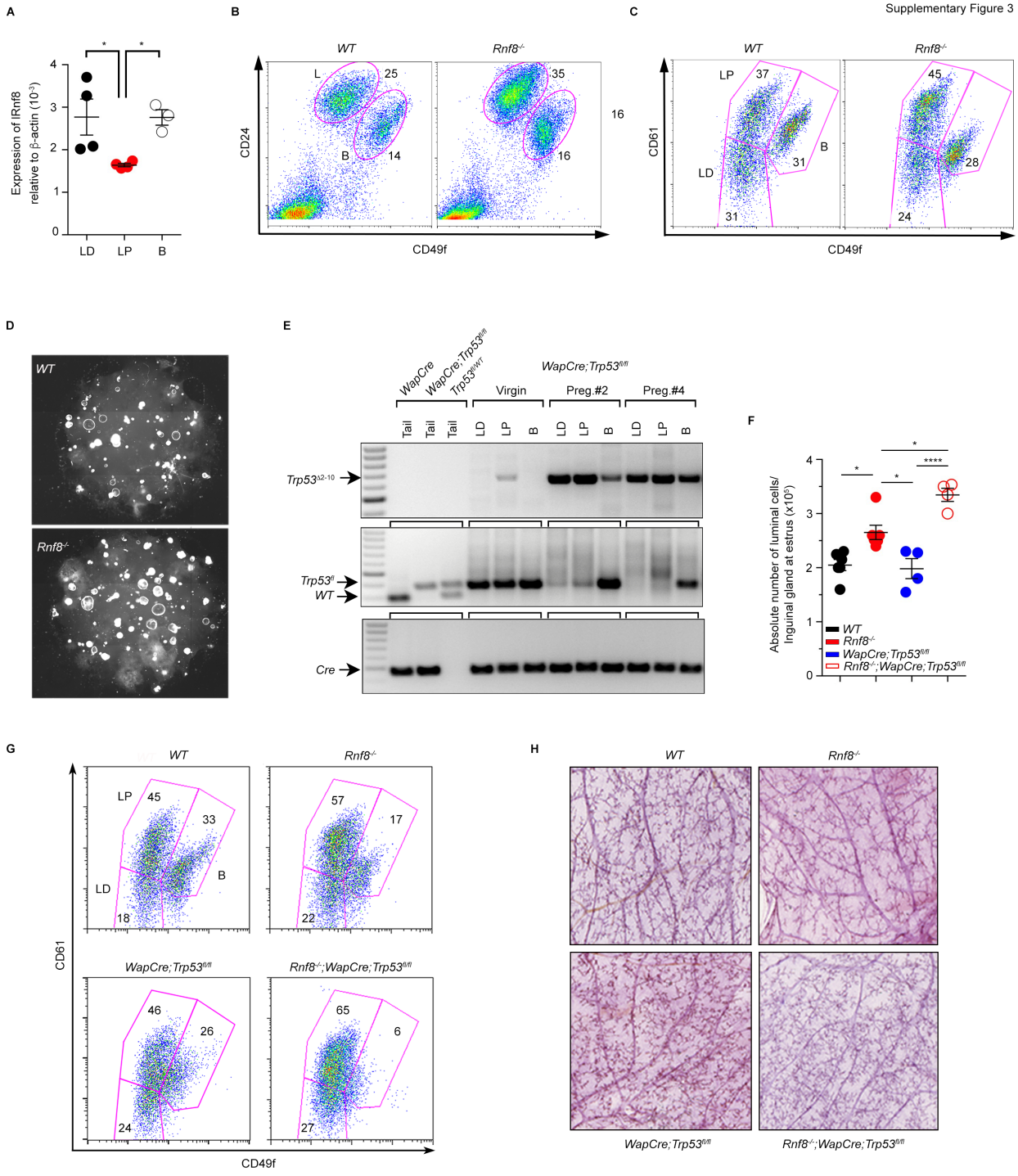

Figure S3. The aberrant expansion of mammary luminal lineage in *Rnf8*$^{-/-}$ females is exacerbated by additional loss of TRP53.

(**A**) qRT-PCR analysis of the expression of Rnf8 in luminal differentiated (LD), luminal progenitor (LP) and basal (B) cell-sorted subpopulations from mammary glands of 3 to 4 *WT* females at estrus phase mean (mean ± SEM). * P<0.05, by 1-way ANOVA followed by Dunnett's test. (**B**)

Representative FACS plots showing Lin$^-$ (CD45$^-$CD31$^-$TER119$^-$) luminal cells (L: CD49f^{low}CD24$^+$) and basal cells (B: CD49f^{high}CD24$^+$) of inguinal mammary glands from *WT* and *Rnf8*$^{-/-}$ littermate females. (**C**) CD49f^{low}CD24$^+$ luminal mammary epithelial cells from (**B**) were further analyzed for luminal progenitor (LP, Lin$^-$CD49f^{low}CD24$^+$CD61$^+$) cells and luminal differentiated (LD, Lin$^-$CD49f^{low}CD24$^+$CD61$^-$) cells. Data are representative of three independent experiments. (**D**) Representative composite tiled images of Matrigel droplets harboring *WT* and *Rnf8*$^{-/-}$ mammary colonies at day 12 of culture. Data are representative of three independent experiments. (**E**) Analysis of WapCre-mediated *Trp53* deletion in cell sorted mammary epithelial subpopulations. PCR analysis of *Cre* and *Trp53* in tail DNA from controls (*WapCre*, *WapCre;Trp53*$^{fl/fl}$, and *Trp53*$^{fl/WT}$ females), as well as DNA from cell sorted LD, LP, and basal cells (B) from *WapCre;Trp53*$^{fl/fl}$ females either virgin or post 2 or 4 pregnancies and involution. All females were at the estrus phase. Tail DNAs from *WapCre*, *WapCre;Trp53*$^{fl/fl}$, and *Trp53*$^{fl/WT}$ females were used as controls. *Cre* PCR was used as loading controls. (**F**) Dot plots depicting the absolute number of luminal cells per inguinal mammary gland from females with the indicated genotypes (n=4 each), at estrus phase (mean ± SEM). All females had undergone 4 pregnancies and involution. * P<0.05, **** P<0.0001 by 1-way ANOVA followed by Tukey's test. (**G**) Representative FACS plots showing % of LP, LD, and basal (B) cells (gated from **Figure 4I**) of mammary glands from 6.5-month-old females as indicated (n=4 each) that have undergone 4 pregnancies and involution to induce Cre-mediated deletion of *Trp53*. All females were at the estrus phase. (**H**) Carmine-alum whole mount analysis of the respective axillary mammary glands from the same female mice in (**F, G**) revealed the absence of hyperplasia (n=4 each).

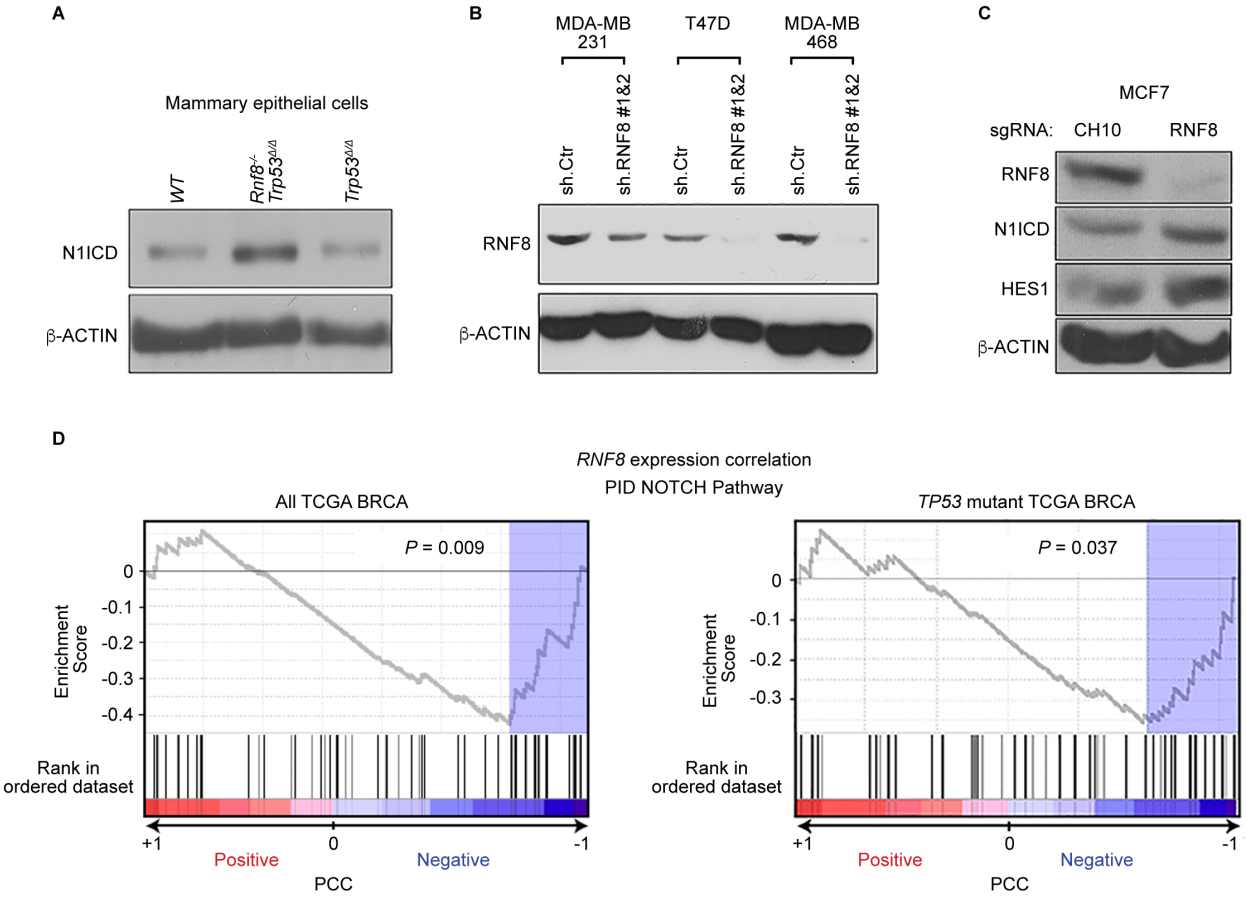

Figure S4. RNF8 deficiency activates Notch signaling in mammary epithelial cells and breast cancer.

(**A**) Immunoblot showing the expression level of N1ICD in mammary epithelial cells from *WT*, *WapCre;Trp53*$^{fl/fl}$ (*Rnf8*$^{-/-}$*Trp53*$^{\Delta/\Delta}$), and *WapCre;Trp53*$^{fl/fl}$ (*Trp53*$^{\Delta/\Delta}$) female mice. Three independent experiments were performed. (**B**) Immunoblot showing RNF8 expression level in *RNF8* knocked down (sh.RNF8#1 and #2) and control (sh.Ctr) MDA-MB-231, T47D and MDA-MB-468 cells. Samples were run on parallel gels contemporaneously. Three independent experiments were performed. (**C**) Immunoblot showing the expression level of RNF8, N1ICD and HES1 in MCF7 cells depleted of endogenous RNF8 using CRISPR/Cas9 (sgRNA-RNF8) and their controls (sgCh10). Three independent experiments were performed. (**D**) Negative expression correlation between *RNF8* and genes encoding for Notch signaling pathway components. GSEA results for the PCCs between *RNF8* and any other gene in the TCGA breast cancer dataset. Left panel, PCC rank using all tumors; right panel, PCC rank using only *TP53* mutant tumors. The tested gene set corresponds to Notch pathway annotation of the NCI Pathway Interaction Database (PID). The graphs include the enrichment scores and the corresponding association *P* values. The pre-ranked GSEA algorithm was run with default parameters and the normalized gene-centered RNAseq TCGA data were downloaded from cBioPortal.

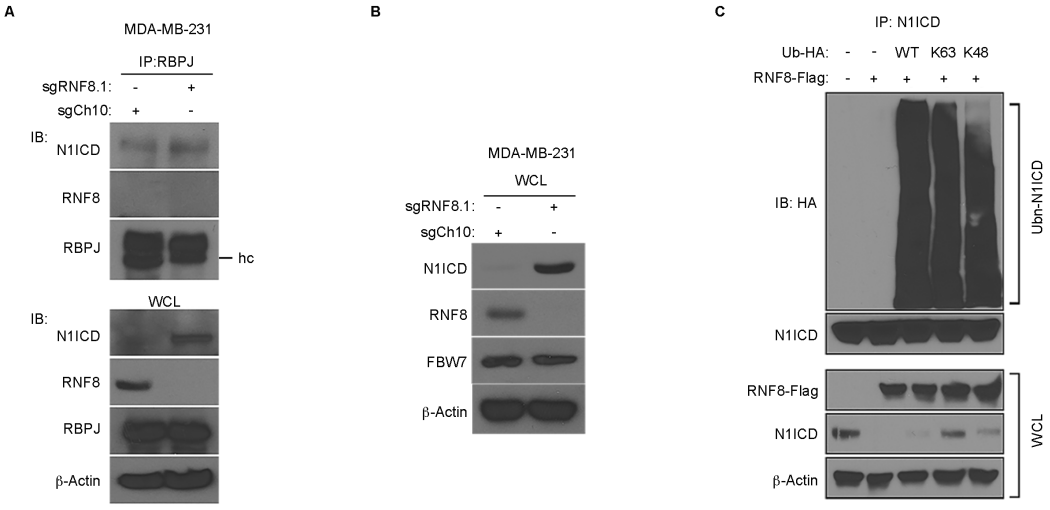

Figure S5. RNF8 ubiquitylates N1ICD to control its turnover.

(**A**) Immunoprecipitated RBPJ and whole cell lysates from the specified MDA-MB-231 cells were immunoblotted as indicated. (**B**) RNF8 deficient (+sgRNF8.1) and control (+sgCh10) MDA-MB-231 cells were examined by immunoblotting for the expression of FBW7, N1ICD and RNF8 as indicated. (**C**) Polyubiquitylation of N1ICD by RNF8. HEK293T cells were transfected as indicated and subjected to immunoprecipitation with anti-N1ICD followed by immunoblotting with the indicated antibodies. (**A**-**C**) At least three independent experiments were performed. IB: Immunoblot. WCL: Whole cell lysate. hc: Immunoglobulin heavy chain.

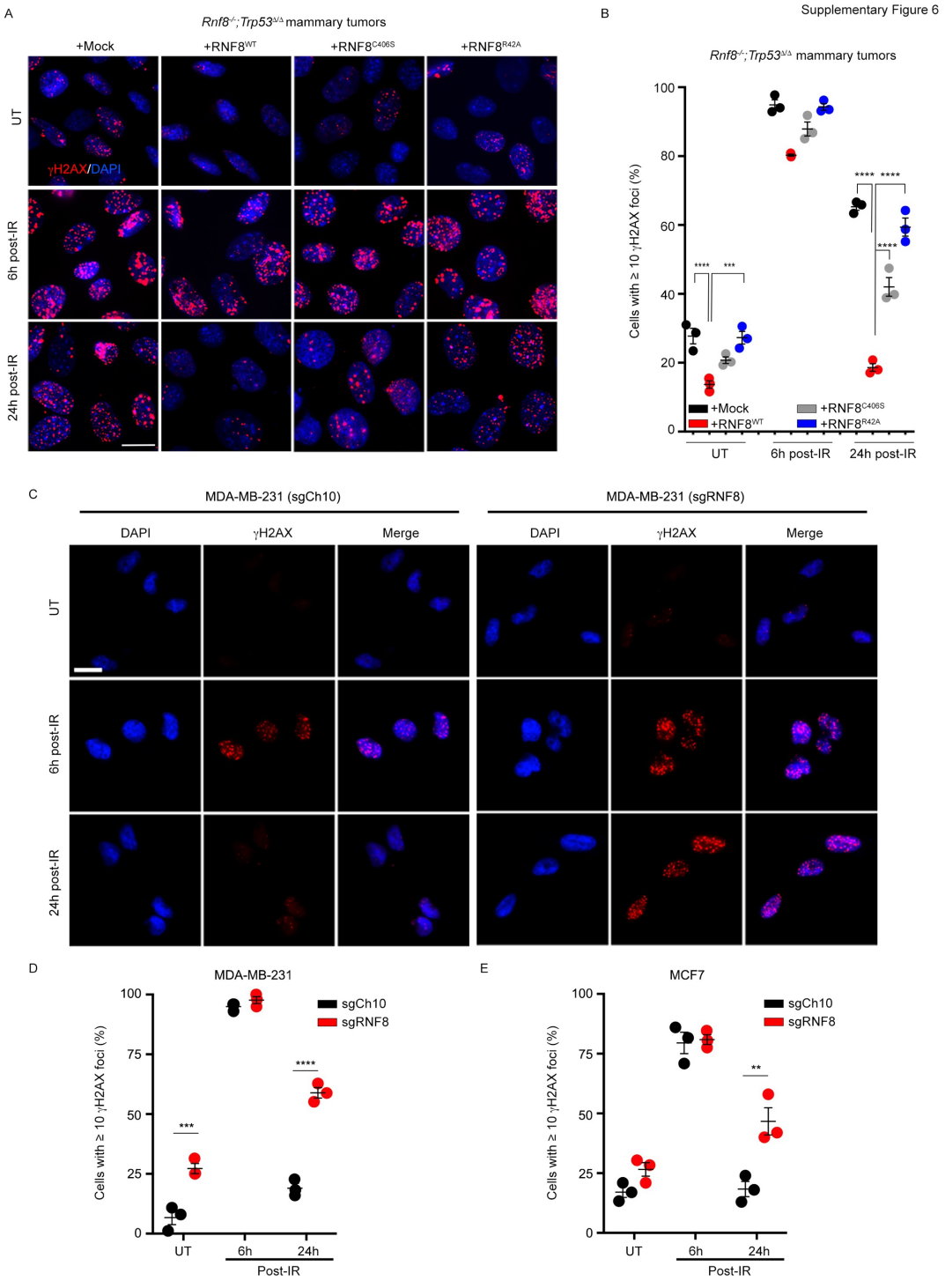

Figure S6. RNF8 is important for DSB repair in human breast cancer cells and both its Ring finger and FHA domains are required the repair function of this E3 ligase.

(**A**) Representative images of γH2ax subnuclear foci formation either spontaneous (UT) or 6h and 24h post-IR (5Gy) of *Rnf8*$^{-/-}$*;Trp53*$^{\Delta/\Delta}$ mammary tumor cells reconstituted with empty vector

(Mock), $RNF8^{WT}$, $RNF8^{C406S}$ or $RNF8^{R42A}$. (**B**) Dot plots depicting quantifications of γH2AX subnuclear foci formation observed in (**A**). Tumor cells harboring ≥10 foci were counted as foci-positive. Three independent experiments were performed, and more than 100 cells were counted for each condition and genotype (mean ± SEM). *** $P<0.001$, **** $P<0.0001$ by 1-way ANOVA followed by Tukey's test. (**C-E**) MDA-MB-231 (**C** and **D**) and MCF7 (**E**) breast cancer cells depleted of endogenous RNF8 using CRISPR/Cas9 (sgRNF8) and their controls (sgCh10) were either left untreated (UT) or harvested at the indicated time-points post-IR (5Gy) and stained with anti-γH2AX antibody and counterstained with DAPI. Representative images of three independent experiments are shown for MDA-MB-231 (**C**). Dot plots showing quantification of γH2AX foci for MDA-MB-231 (**D**) and MCF7 (**E**). Data are presented as mean ± SEM of three independent experiments and more than 100 cells for each condition and genotype were counted. Bar: 20μm for **A** and **C**. (**D**, **E**) ** $P<0.01$, *** $P<0.001$, **** $P<0.0001$ by 1-way ANOVA followed by Tukey's test.

Table S1: Names and sequences of RT-PCR primers.

Gene	Forward primer	Reverse primer
Mouse *Hes1*	AAAGCCTATCATGGAGAAGAGGCG	GGAATGCCGGGAGCTATCTTTCTT
Mouse *Hey1*	ACACTGCAGGAGGGAAAGGTT	CAAACTCCGATAGTCCATAGCCA
Mouse *Slug*	GATGTGCCCTCAGGTTTGAT	ACACATTGCCTTGTGTCTGC
Mouse *Ccnd1*	GCGTACCCTGACACCAATCTC	ACTTGAAGTAAGATACGGAGGGC
Mouse *FoxM1*	GAGGAAAGAGCACCTTCAGC	AGGCAATGTCTCCTTGATGG
Mouse *p18*	TTATGAAGCACACAGCCTGCAATGT	ACGGACAGCCAACCAACTAACGG
Mouse *Ccnd2*	GAGTGGGAACTG GTAGTGTTG	CGCACAGAGCGATGAAGGT
Mouse *c-Myc*	TGAGCCCCTAGTGCTGCAT	TCCACAGACACCACATCAATTTC
Mouse *Hif1α*	ACCTTCATCGGAAACTCCAAAG	CTGTTAGGCTGGGAAAAGTTAGG
Mouse *Adam17*	ACCACTTTGGTGCCTTTCGT	GTCGCAGACTGTAGATCCCTT
Mouse *Hdac2*	GGAGGAGGCTACACAATCCG	TCTGGAGTGTTCTGGTTTGTCA
Mouse *Numbl*	GCAGGCACCATGAACAAGTTA	TCTTCACAAACGTGCATTCCC
Mouse *Fhl1*	GACTGCCGCAAGCCCATAA	CCAAGGGGTGAAGGCACTT
Mouse *Gapdh*	AAGGTCATCCCAGAGCTGAA	CTGCTTCACCACCTTCTTGA
Mouse *β-Actin*	CCATACCCAAGAAGGAAGGCT	TATTGGCAACGAGCGGTTC
Human *HES1*	TACTTCCCCAGCACACTTGG	CGGACATTCTGGAAATGACA
Human *HES2*	CCAACTGCTCGAAGCTAGAGA	AGCGCACGGTCATTTCCAG
Human *HEY1*	CGAAATCCCAAACTCCGATA	TGGATCACCTGAAAATGCTG
Human *HEY2*	GGCACTCTCGGAATCCTATG	TTTGAAGATGCTTCAGGCAA
Human *CCND1*	CCGTCCATGCGGAAGATC	GAAGACCTCCTCCTCGCACT
Human *GAPDH*	CCACTCCTCCACCTTTGAC	ACCCTGTTGCTGTAGCCA
Human *β-ACTIN*	TGACCCAGATCATGTTTGAGA	AGAGGCGTACAGGGATAGCA